Collisional Stabilization and Thermal Dissociation of Highly Vibrationally Excited $C_9H_{12}^+$ Ions from the Reaction $O_2^+ + C_9H_{12} \rightarrow O_2 + C_9H_{12}^{+\dagger}$

Abel I. Fernandez,[‡,§] A. A. Viggiano,*[,‡] Thomas M. Miller,[‡] S. Williams,[‡] I. Dotan,[||] J. V. Seeley,[⊥] and J. Troe[#]

Air Force Research Laboratory, Space Vehicles Directorate, 29 Randolph Road, Hanscom AFB, Massachusetts 01731-3010, NRC Research Associateship Program, Keck Center of the National Academies, 500 Fifth Street, NW, GR 322A, Washington, D.C. 20001, Department of Natural Sciences, The Open University of Israel, Ramat Aviv, Tel Aviv, Israel, Department of Chemistry, Oakland University, Rochester, Michigan 48309-4401, and Institute for Physical Chemistry, University of Goettingen, Tammannstrasse 6, D-37077 Goettingen, Germany

Received: April 29, 2004; In Final Form: July 8, 2004

Highly vibrationally excited *n*-propylbenzene cations, $C_9H_{12}^+$*, were prepared by the charge transfer reaction $O_2^+ + C_9H_{12} \rightarrow O_2 + C_9H_{12}^+$* in a turbulent ion flow tube. The subsequent competition between fragmentation of $C_9H_{12}^+$* into $C_7H_7^+ + C_2H_5$ and stabilization in collisions with N_2 was studied at temperatures in the range 423−603 K and at pressures between 15 and 200 Torr. Most of the $C_7H_7^+$ is the aromatic benzylium isomer, while the fraction of the minor species, seven-membered-ring tropylium, increases with *T*, from 5 to 20%. Minor fragments are $C_6H_6^+$, $C_7H_8^+$, and $C_8H_9^+$. Energy-transfer step sizes $\langle\Delta E\rangle$ for collisional deactivation are obtained by combining the stabilization versus fragmentation ratios measured as a function of pressure in this study with fragmentation rates from the literature. The values are compared with related information for other excited molecular ions and are similar to those of their neutral analogues. At the highest temperatures, $C_9H_{12}^+$ was also observed to pyrolyze after collisional stabilization. Employing unimolecular rate theory, the derived rate constants for thermal dissociation of $C_9H_{12}^+$ are related to values derived from the specific rate constants $k(E,J)$ for fragmentation. Good agreement is found between measured and predicted pyrolysis rate constants. This allows us to confirm the dissociation energy of $C_9H_{12}^+$ into $C_7H_7^+$ (benzylium) and C_2H_5 as 166.9 (±2.2) kJ mol^{-1} (at 0 K).

1. Introduction

Charge transfer can generate chemically activated molecular ions which subsequently undergo a variety of reactive and nonreactive processes. Reactive processes include dissociation at high excitation energies and secondary reactions. The unreactive or energy-dissipative processes include collisional stabilization and radiative cooling of vibrationally excited molecular ions. At high temperatures, the stabilized molecules subsequently undergo thermal dissociation.

In previous work, we have generated highly vibrationally excited alkylbenzene cations by charge transfer from small ions to alkylbenzenes in a high-temperature flowing afterglow (HTFA) and in a selected ion flow tube (SIFT).[1−3] Branching ratios were determined as a function of the temperature, and mechanisms were determined. The comparison of charge transfer breakdown curves taken at about 1 Torr to data from low-pressure photodissociation experiments suggested that the buffer gas had an influence by either collisionally stabilizing and/or thermally dissociating the ions. The small pressure variation (at most 0.2−1 Torr), however, did not allow for a systematic analysis of pressure effects. The subsequent construction of a high-pressure turbulent ion flow tube[4,5] (TIFT), operating at buffer gas pressures from 15 up to 700 Torr, allows us to better investigate pressure dependences. Recent improvements to the TIFT allow measurements over a broader temperature range than in previous studies. Studies of this type, for example, the reaction of O_2^+ with ethylbenzene, allowed for an investigation of the competition between unimolecular fragmentation of ethylbenzene cations (forming methyl radicals and $C_7H_7^+$ isomers: the aromatic benzylium and the seven-membered-ring tropylium ions[6]) and collisional stabilization of the excited ethylbenzene ions.[7] Since the specific rate constants $k(E)$ for fragmentation are known from separate absolute rate measurements,[8,9] the effective rates for collisional stabilization could be deduced.[7] These results were analyzed in a simplified master equation approach[10] leading to the product of the total collision frequency, *Z*, and average step size for deexcitation, $\langle\Delta E\rangle$, at each temperature. $\langle\Delta E\rangle$ values were obtained by identifying *Z* as the ion-induced dipole capture rate constant. The $\langle\Delta E\rangle$ values were found to be similar to those for the corresponding neutral alkylbenzenes.

Little information exists on collisional energy transfer from molecular ions which are highly vibrationally excited. While relative collision efficiency measurements are available,[11−13] it is difficult to put them on an absolute scale of energy transfer rates. Since our O_2^+ + ethylbenzene experiments[7] have led to values of the product $Z\langle\Delta E\rangle$, it appears desirable to derive similar information also for other excited polyatomic ions.

This is the aim of the present series of articles in which experiments for the reactions of O_2^+ with *n*-propylbenzene (this work) and with *n*-butylbenzene[14] are described. A second goal of the our work is to study the pyrolysis of the stabilized

† Part of the special issue "Tomas Baer Festschrift".
‡ Air Force Research Laboratory.
§ NRC Research Associateship Program.
|| The Open University of Israel.
⊥ Oakland University.
University of Goettingen.

10.1021/jp048132s CCC: $27.50
Published on Web 10/05/2004

alkylbenzene ions and to attempt to relate specific rate constants $k(E)$ for fragmentation with the derived thermal dissociation rate constants. The present work, involving *n*-propylbenzene ions, presents this approach for the first time.

The chemistry of the $O_2^+ + n$-propylbenzene (C_9H_{12}) system involves numerous processes:[15]

$$O_2^+ + C_9H_{12} \rightarrow O_2 + C_9H_{12}^+* \qquad k_1 \qquad (1.1)$$

$$C_9H_{12}^+* \rightarrow C_7H_7^+ (Bz^+) + C_2H_5 \qquad k_2 \qquad (1.2)$$

$$C_9H_{12}^+* \rightarrow C_7H_7^+ (Tr^+) + C_2H_5 \qquad k_3 \qquad (1.3)$$

$$C_9H_{12}^+* + M \rightarrow C_9H_{12}^+ + M \qquad k_4 \qquad (1.4)$$

$$C_9H_{12}^+* \rightarrow C_9H_{11}^+ + H \qquad k_5 \qquad (1.5)$$

$$C_9H_{12}^+* \rightarrow C_8H_9^+ + CH_3 \qquad k_6 \qquad (1.6)$$

$$C_9H_{12}^+* \rightarrow C_6H_6^+ + C_3H_6 \qquad k_7 \qquad (1.7)$$

(Bz^+ denotes benzylium, Tr^+ is tropylium). Channels 1.3 and 1.5−1.7 are minor under the present conditions and can be mostly ignored. The bulk of this article focuses on reactions 1.1, 1.2, and 1.4. In addition, at temperatures approaching 600 K, collisionally stabilized $C_9H_{12}^+$ ions can pyrolyze,

$$C_9H_{12}^+(+M) \rightarrow C_7H_7^+ + C_2H_5(+M) \qquad k_8 \qquad (1.8)$$

Secondary reactions occur but are accounted for by extrapolating to zero $[C_9H_{12}]$.

There is also a practical aspect to the measurements. The bottleneck for combustion of hydrocarbon fuels often is the ignition delay caused by the primary fragmentation of the fuel molecules. Injection of radicals or ions can considerably speed up the ignition and may be required for advanced hydrocarbon-fuelled airbreathing propulsion systems.[1] The present work contributes to this practical aspect of combustion technology under conditions more appropriate to real life engines.

2. Experimental Technique

Our experiments were conducted in the TIFT which has been described in detail before;[4,16] therefore the technique is only briefly summarized here. The TIFT is similar to low-pressure flow tubes except that larger flow rates are used to achieve higher pressures and Reynolds numbers. A liquid nitrogen storage vessel supplies the N_2 carrier gas, which is preheated in a sidearm. The ions are created upstream in an off-axis corona discharge source and are entrained into the N_2 flow in the sidearm. The gas enters the flow tube where the neutral reagent is injected through a moveable on-axis tube. At the end of the flow tube, most of the gas is removed by a large mechanical pump while a small fraction is sampled through a 150 μm orifice in a truncated nose cone. The core of the ensuing supersonic expansion is sampled through a skimmer into a mass spectrometer. The ions are analyzed by a quadrupole mass filter and counted by a discrete dynode electron multiplier.

To elevate the temperature, six zones of heating are used and the thermocouple that monitors the gas temperature is maintained to ±2 K. The main flow tube is heated in four zones, two short zones at either end, a long middle section, and a zone inside the vacuum chamber just upstream of the nose cone. The connection between the corona discharge tube and the sidearm is also heated. Last, it was found that preheating of the buffer gas is needed. During the course of this work, the preheater design was changed to allow for higher temperatures. The new preheater consists of two Mellen split type (clam shell) tubular heating elements that surround a tubular piece of copper; the gas flows through narrow channels (which traverse the copper tube along the axis) that have a radial-spoke cross section. The pattern was chosen to promote efficient heating.

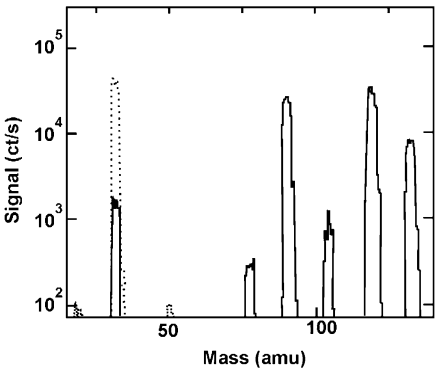

Figure 1. Typical low-resolution mass spectrum of the $O_2^+ + C_9H_{12}$ system. The dashed peak at mass 32 corresponds to the undepleted O_2^+ signal before the addition of propylbenzene. The peak at mass 133 corresponds to a secondary reaction of benzylium ($C_7H_7^+$) with C_9H_{12}; see eq 2.1.

A typical mass spectrum is shown in Figure 1, with and without the propylbenzene reactant gas. In the absence of propylbenzene, the O_2^+ signal is dominant (>99%).

Common impurities are $H_3O^+(H_2O)_{0,1}$ and $O_2^+(H_2O)$. Since the relative concentrations of the impurities were usually less than 2% (sometimes much less), no corrections to the recorded branching ratios were made. When propylbenzene is added, ions at 78, 91, 92, 105, 120, and 133 amu are observed. In Figure 1, the 92 amu peak is hidden in the large 91 amu peak. Higher resolution spectra are used to separate the two peaks, and an isotope correction is made. The mass 78 and 105 amu peaks are present at the same levels as impurities, ca. 0.5−2% at low temperatures. At higher temperatures, their yields increase and can be investigated. The dissociative and nondissociative charge transfer products at 91 and 120 amu, respectively, dominate. The peak at mass 133 is due to a reaction between benzylium and propylbenzene[3], that is,

$$C_7H_7^+(Bz^+) + C_9H_{12} \rightarrow C_{10}H_{13}^+ + C_6H_6 \qquad (2.1)$$

Branching ratios of the ion products were recorded as a function of the neutral reagent concentration. Secondary chemistry was taken into account by extrapolating to zero concentration. The accessible temperature and pressure ranges were limited by the allowable intensity of impurity ions (<2%) at low T and high P, thermal decomposition of $C_9H_{12}^+$ at high T, and small signals at low P.

Up to 523 K, the pyrolysis reaction 1.8 could be neglected. In this case, the mass 120 versus 91 ratio, which we call S/D, can be symbolically written as

$$\frac{S}{D} = \frac{[C_9H_{12}^+]}{[C_7H_7^+]} = \frac{k_4[M]}{k_2 + k_3} \qquad (2.2)$$

Here it is assumed that at zero pressure, all of the $C_9H_{12}^+$ dissociates, but in section 3, it is shown that the S/D values exhibit a nonzero intercept at low pressures, indicating that some of the $C_9H_{12}^+$ transfer product is stable at zero pressure. Minor

channels are excluded in the dissociation signal. At $T \geq 573$ K, S/D values vary with the injector position and therefore time, indicating that thermal decomposition of $C_9H_{12}^+$ is occurring.

Our first attempt to determine the pyrolysis rate of $C_9H_{12}^+$ involved direct observation of the depletion of $C_9H_{12}^+$ as a function of distance by using NO^+ or $C_6H_6^+$ as reagent ions. Because the ionization potentials of C_6H_6, NO, and C_9H_{12} are similar,[17] this avoided the unwanted presence of highly vibrationally excited $C_9H_{12}^+$. Unfortunately, this approach yielded uninterpretable results and was abandoned. Explanations for the failure include interference from the isomerization of the benzene cation to the five-membered-ring species, fulvene,[18] and hydrogen abstraction reactions when NO^+ was used as the charge transfer agent.

The method that was successful involves the deconvolution of the effects of time and pressure. An advantage over the previous method is that (S/D) in the absence of thermal decomposition ($t = 0$), called $(S/D)_0$, can also be obtained. S/D was measured in the usual way at several distances (i.e., reaction times) at the same T and P. This was repeated at numerous pressures, $P = 30-250$ Torr, at 573 and 603 K.

A steady-state solution of the kinetics, modeled by eqs 1.1−1.4 and 1.8 which include stabilization, dissociation, and thermal dissociation, yields

$$\frac{S}{D} \approx \frac{\dfrac{k_4[M]}{(k_2+k_3)}[1-\exp(-k_8 t)]}{k_8 t\left(1+\dfrac{k_4[M]}{(k_2+k_3)}\right)-\left(\dfrac{k_4[M]}{(k_2+k_3)}\right)[1-\exp(-k_8 t)]} \quad (2.3)$$

Minor channels are neglected. Extrapolating to zero time leads back to eq 2.2, as expected; this value is $(S/D)_0$. At high temperatures and nonzero time, substitution of eq 2.2 into eq 2.3 yields the following:

$$\frac{S}{D} \approx \frac{(S/D)_0[1-\exp(-k_8 t)]}{k_8 t(1+(S/D)_0)-(S/D)_0[1-\exp(-k_8 t)]} \quad (2.4)$$

We assume that the decrease of the product of concentrations $[C_9H_{12}][O_2^+]$ during the course of the reaction is insignificant since we extrapolate to zero extent of reaction. Nonlinear least-squares fits of the time dependence of S/D at each pressure to eq 2.4 yield both k_8 and $(S/D)_0$. Note that this involves both an extrapolation to $[C_9H_{12}] = 0$ and the fit to the time dependence, thereby introducing noticeable scatter in the data. The fitted k_8 values at 573 K varied by a factor of 2. The scatter at 603 K is less since the pyrolysis rate is larger. The factor of 2 scatter is an estimate of the accuracy. Figure 2 shows a typical time dependence of S/D at $T = 573$ and 603 K and at a nitrogen pressure of 100 Torr. The pyrolysis decay is easily detected. We, therefore, have the interesting situation of a chemical activation process which is initiated by a charge transfer reaction and which, after collisional stabilization of the highly excited products, is followed by thermal dissociation of the stabilized species. The intrinsic kinetics of chemical activation and thermal dissociation is connected and must be interpreted in a consistent way, and this is done here.

The fragmentation of $C_9H_{12}^+$* is known to lead to two isomers of $C_7H_7^+$, Bz^+ and Tr^+.[15] The former contains the six-membered aromatic ring and is reactive with propylbenzene to produce $C_9H_{11}^+$ (mass 119) and $C_{10}H_{13}^+$ (mass 133) via reaction 2.1. By contrast, the latter is comprised of an unreactive seven-membered ring. This difference in reactivity allows for the Tr^+ yield to be measured by alternately using low and high propylbenzene flows. Low concentrations of propylbenzene are used to measure the total relative concentration of $C_7H_7^+$, whereas at high concentrations Bz^+ is completely removed. Subtraction of the two limits yields the amount of Bz^+. At 423 K, the Tr^+ yield was found to be about 1%, and at 523 K the value was roughly 7%. At 573 K, a yield around 20% was found. The uncertainty is considerable since the propylbenzene cation starts to decompose at this temperature and the kinetics of reaction 2.1 has not been measured at high temperature.

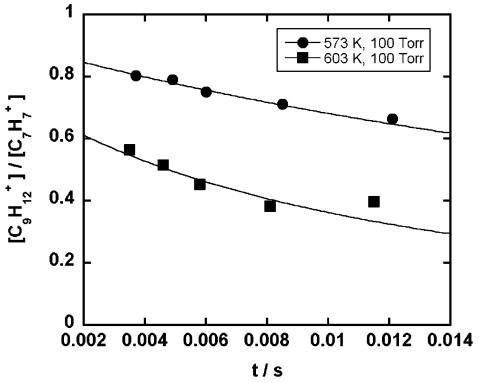

Figure 2. Thermal decomposition of $C_9H_{12}^+$. $[C_9H_{12}^+]/[C_7H_7^+]$ is plotted vs reaction time at pressures of 100 Torr of N_2. Best fits to eq 2.4, shown as curves, yield values of $(S/D)_0$, the ratio of stabilization to dissociation in the absence of thermal decomposition, and k_8, the first-order thermal decomposition rate coefficient of $C_9H_{12}^+$.

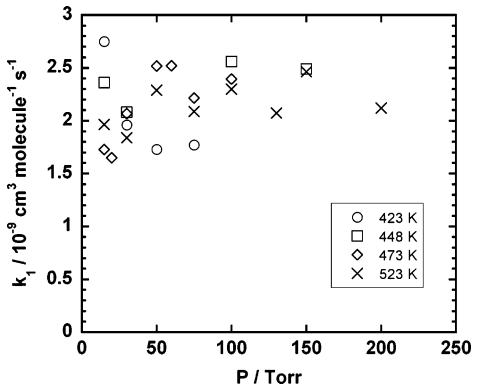

Figure 3. Rate constants k_1 for the reaction of O_2^+ with C_9H_{12} as a function of pressure at various temperatures.

3. Results

The experimental results are of three types: (1) the total rate constant k_1 of the charge transfer process 1.1, (2) branching ratios as a function of temperature and of pressure (mostly the ratio of $C_9H_{12}^+$ to $C_7H_7^+$ but the other channels are also reported), and (3) the thermal decomposition rate constants at high temperature as a function of pressure. Rate constants k_1 are plotted in Figure 3, and S/D values are listed in Table 1. Table 2 lists the thermal decomposition rates, and Table 3 lists the ratio of mass 91 to the minor products and to the fraction of mass 91 that is tropylium.

The rate constants shown in Figure 3 show no dependence of k_1 on temperature or pressure over the ranges 423−523 K and 30−200 Torr. The uncertainty of individual rate constants was about ±25%. Part of the scatter is because most of the effort was focused on the more interesting branching information where low depletion is used. Rate constants are better obtained under high depletion. The average value of all measurements

TABLE 1: Stabilization vs Dissociation Yields S/D = $[C_9H_{12}^+]/[C_7H_7^+]$ in N_2[a]

T/K	*P*/Torr	$[N_2]$	S/D	c_1	c_2
423	15	0.31	1.18	0.59	1.44
	30	0.65	1.61		
	50	1.15	2.28		
	75	1.69	3.18		
448	15	0.29	1.07	0.86	0.516
	30	0.62	1.07		
	50	1.05	1.43		
	75	1.58	1.69		
	100	2.11	1.94		
	150	3.19	2.22		
473	15	0.28	0.87	0.79	0.323
	30	0.60	0.96		
	50	0.99	1.13		
	75	1.51	1.29		
	100	2.03	1.48		
	150	3.04	1.74		
523	15	0.26	0.75	0.68	0.134
	30	0.54	0.66		
	50	0.92	0.83		
	75	1.37	0.86		
	100	1.81	1.00		
573	30	0.505	0.63	0.54	0.147
	50	0.835	0.67		
	75	1.26	0.82		
	100	1.68	0.90		
	150	2.52	0.95		
	200	3.35	1.08		
	250	4.19	1.36		
603	30	0.474	0.46	0.48	0.0599
	50	0.798	0.54		
	75	1.19	0.65		
	100	1.59	0.72		
	150	2.39	0.66		
	200	3.19	0.92		
	250	4.00	1.32		

[a] $[N_2]$ in 10^{18} molecule cm^{-3}, c_2 in 10^{-18} molecule^{-1} cm^3.

TABLE 2: Thermal Dissociation Rate Constants k_8 for $C_9H_{12}^+ \rightarrow C_7H_7^+ + C_2H_5$

T/K	*P*/Torr	k_8/s^{-1}	*T*/K	*P*/Torr	k_8/s^{-1}
573	30	75	603	30	101
	50	37		50	109
	75	44		75	109
	100	32		100	98
	150	22		150	75
	200	27		200	109
	250	34		250	138

was found to be $k_1 = 2.1 \times 10^{-9}$ cm^3 molecule^{-1} s^{-1}, in agreement with our previous measurements,[1,3] and confirms the accuracy of the TIFT approach. This value is also in good agreement with the Langevin rate constant for capture of C_9H_{12} by O_2^+, which is calculated as $k_L = 1.89 \times 10^{-9}$ cm^3 molecule^{-1} s^{-1} on the basis of an estimated[19] polarizability of C_9H_{12} of $\alpha = 16.1 \times 10^{-24}$ cm^3 (contributions from polarizability anisotropies and quadrupole and permanent dipole moments at this level can be neglected).

The measurements of S/D (or $(S/D)_0$ at higher temperatures) are presented in Table 1 and plotted as a function of the temperature and the buffer gas concentration in Figure 4. The data show that lower temperatures and higher pressures favor the formation of the nondissociative product, that is, give larger S/D. The measurements exhibit a roughly linear dependence on $[N_2]$ or equivalently pressure. One also notices an apparent intercept of the S/D versus $[N_2]$ curves as $[N_2] \rightarrow 0$ which is in contrast to the predictions from eq 2.2.

The present results are similar to our previous observations for the O_2^+ + ethylbenzene reaction. The intercept indicates that there is a fraction, α, of reaction 1.1 that leads to

TABLE 3: Ratio of Concentrations of Major- to Minor-Ion Fragments from the Reaction $O_2^+ + C_9H_{12} \rightarrow C_7H_7^+ +$ Other (Minor) Ion Fragments

T/K	*P*/Torr	$[C_7H_7^+]/[C_7H_8^+]$	$[C_7H_7^+]/[C_6H_6^+]$	$[C_7H_7^+]/[C_8H_9^+]$	$[Tr^+]/[C_7H_7^+]_{tot}$[a,b]
423	15	17.8	23.0	51.0	0.010
	30	16.3	25.9	64.8	
	50	18.2	28.4	78.0	
	75		39.8	60.0	
448	15	16.1			
	30	15.2	20.3		
	50	16.7	23.1	83.0	
	75	17.3	26.9	75.4	
	100	19.6	26.5	69.0	
	150	18.3	28.8	79.3	
473	15		25.0	40.4	0.010
	30	18.5	22.0	63.3	
	50	14.8	24.8	67.3	
	75	18.8	25.8	87.8	0.041
	100	21.3	25.4	67.8	0.030
	150	16.4		93.5	
	200	16.1			
523	15	16.4	19.1	25.2	0.032
	30	16.3	21.9	53.6	
	50	17.8	20.8	60.1	0.091
	75	18.3	25.5	76.4	
	100	18.9	23.7	62.3	
	150	25.8	20.0	53.6	0.070
	200	21.1	18.4	65.9	

[a] Fraction of Tr^+, the seven-membered-ring tropylium isomer of $C_7H_7^+$; the aromatic benzylium isomer is the major species. [b] Data of $[Tr^+]/[C_7H_7^+]_{tot}$ at 573 K, about 18% and invariant from 30 to 200 Torr, are not included here due to interference from thermal decomposition.

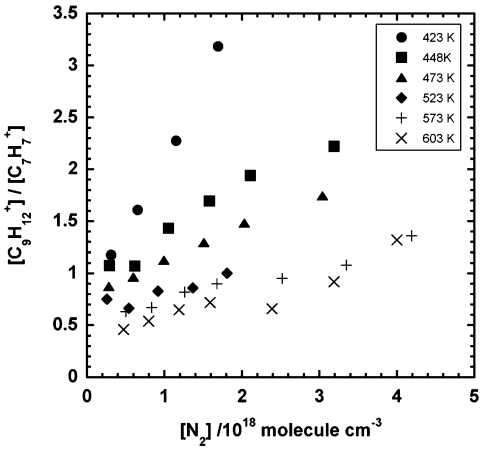

Figure 4. Ratio of stabilization to decomposition vs $[N_2]$. Temperatures range from 423 to 603 K, while pressure was varied from about 15 to 250 Torr. At $T \geq 573$ K, thermal decomposition is considerable and is taken into account.

nondissociative products. Therefore, the mechanism of reactions 1.1−1.8 is extended to (excluding minor channels)

$$O_2^+ + C_9H_{12} \rightarrow O_2 + C_9H_{12}^+ \qquad \alpha k_{cap} \qquad (3.1)$$

$$O_2^+ + C_9H_{12} \rightarrow O_2 + C_9H_{12}^+* \qquad (1-\alpha)k_{cap} \qquad (3.2)$$

$$C_9H_{12}^+* \rightarrow C_7H_7^+ + C_2H_5 \qquad k(E) \qquad (3.3)$$

$$C_9H_{12}^+* + M \rightarrow C_9H_{12}^+ + M \qquad \gamma_c Z \qquad (3.4)$$

$$C_9H_{12}^+ (+M) \rightarrow C_7H_7^+ + C_2H_5 (+M) \qquad k_8 \qquad (3.5)$$

$C_7H_7^+$ in reaction 3.3 stands for the sum of Bz^+ and Tr^+ but, as shown in Table 3, is mostly the former. *E* denotes the internal energy of the chemically activated propylbenzene cations, and

TABLE 4: Energy Transfer Properties for Highly Excited Propylbenzene Ions[a]

T/K	$k(E)/\gamma_c$ s^{-1}	$I(T)$	γ_c ($T = 0$)	$-\langle\Delta E\rangle/hc$ cm^{-1}
423	7.18×10^8	0.278	0.195	336
448	2.34×10^9	0.240	0.069	119
473	1.12×10^9	0.207	0.168	288
523	2.89×10^9	0.152	0.089	153
573	2.87×10^9	0.110	0.123	212
603	7.33×10^9	0.0905	0.059	101

[a] See the text; analysis with eqs 4.4 and 4.5; $E_{ch}/hc = 27\,030$ cm^{-1}, $k(E_{ch}) = 3.90 \times 10^7$ s^{-1}, $s^* = 7.608$, $Z = 6.5 \times 10^{-10}$ cm^3 molecule^{-1} s^{-1}, c_1 and c_2 from Table 1.

$k(E)$ is the specific rate constant for their fragmentation. We identify Z with the Langevin capture rate constant between $C_9H_{12}^+$ and M: $Z = 6.5 \times 10^{-10}$ cm^3 molecule^{-1} s^{-1}. S/D is represented in this mechanism as

$$\frac{S}{D} = \frac{[C_9H_{12}^+]}{[C_7H_7^+]} \approx \frac{\alpha}{1-\alpha} + \frac{\gamma_c Z[N_2]}{(1-\alpha)k(E)} \qquad (3.6)$$

Linear extrapolations of S/D versus $[N_2]$ in Figure 4 to $[N_2] \rightarrow 0$ yield intercepts on the order of 0.66 for all temperatures giving $\alpha = 0.40$, similar to the value of $\alpha = 0.44$ found in our $O_2^+ + C_8H_{10}$ experiments.[7]

The apparent intercepts in Figure 4 are significantly larger than S/D values observed in our previous measurements[1] of the $O_2^+ + C_9H_{12}$ reaction at lower pressures; for example, measurements in the selected ion flow tube and the high-temperature flowing afterglow at 0.5 Torr of N_2 at 500 K gave S/D = 0.15. Furthermore, experiments from a single-collision guided-ion beam apparatus led to values of S/D = 0.19 and 0.11 at 300 and 650 K, respectively. For $C_8H_{10}^+$, we attributed this "nondissociative" fraction to incomplete energy transfer in some of the charge transfer encounters, which is quenched at lower pressures than studied here. Several types of charge transfer processes were postulated and were analyzed in detail in ref 7. The present work employs an analogous interpretation. The three processes are (1) resonant charge transfer in which the difference of the ionization energies of O_2 and C_9H_{12} into $C_9H_{12}^+$ is transferred, (2) complex formation where the energy transfer is statistical, and (3) resonant charge transfer where the O_2 neutral is produced in an excited state.

The results from Table 1 were fit to a linear expression according to eq 3.5, S/D $\approx c_1 + c_2[N_2]$, and the fit parameters c_1 and c_2 are summarized in Table 1. The values for $k(E)/\gamma_c = Z(1 + c_1)/c_2$ are given in Table 4. $k(E)/\gamma_c$ in this representation corresponds to averages over suitable energy distributions of $C_9H_{12}^+$*. A more detailed analysis is given below.

The rate constant for the thermal dissociation of $C_9H_{12}^+$ has been measured at 573 and 603 K. The average values are $k_8 = 33$ s^{-1} at 573 K and $k_8 = 106$ s^{-1} at 603 K and do not depend on pressure, indicative of the high-pressure limit. Our analysis presented below is in accord with this conclusion. The corresponding Arrhenius expression is $k_8 \approx 5.7 \times 10^{11} \exp(-112$ kJ mol$^{-1}/RT)$ s^{-1}. The factor of 2 uncertainty in the rates and the small temperature range lead to uncertainty on the order of 70 kJ mol^{-1} in the activation energy. If one assumes the activation energy to be the dissociation energy, $E_0 = 167$ kJ mol^{-1},[15] the two values of k_8 correspond to

$$k_8 \approx 2.1\ (\pm 0.9) \times 10^{16} \exp(-167 \text{ kJ mol}^{-1}/RT)\ \text{s}^{-1} \qquad (3.7)$$

While this expression appears more reasonable, an internally consistent derivation of k_8 is given in the discussion section.

All minor channels decrease with increasing pressure (relative to $[C_9H_{12}^+]$). However, the data had too much scatter to ascertain if individual channels had different dependences. No attempt was made to correct these channels for impurities, since the procedure was uncertain. The most abundant of the minor channels is $C_7H_8^+$, which is approximately 5−6% of the $C_7H_7^+$ channel. There is no temperature dependence within our uncertainty, as is true for all minor species. $C_6H_6^+$ and $C_8H_9^+$ are about 4 and 2% of the $C_7H_7^+$ signal, respectively. The Tr^+ is small except in the temperature range where thermal dissociation becomes important, where 20% of $C_7H_7^+$ was observed as tropylium. However, the monitor ion chemistry was not measured at high temperature.

4. Analysis of Experimental Results

4.1. Energy Distributions from Charge Transfer. The observation of S/D values between 0.1 and 0.2 under single-collision conditions indicates that part of the charge transfer reaction 1.1 generates $C_9H_{12}^+$* with very low energy. Either the energy of this fraction is below the dissociation threshold or can be stabilized by radiative cooling in $\sim 10^{-2}$ s. We speculate that this fraction is due to production of electronically excited O_2.[7] The intercepts in Figure 4 are larger than the low-pressure limiting value, providing evidence for a second channel where only partial energy transfer occurs. We suggest that this involves formation of the complex $(O_2{-}C_9H_{12})^+$ which upon dissociation distributes energy statistically between O_2 and $C_9H_{12}^+$. Finally, near-resonant charge transfer deposits the difference between the ionization energies of O_2 and C_9H_{12} into vibrational energy of $C_9H_{12}^+$; at the same time, the thermal energies of O_2^+ and C_9H_{12} are assumed to be nearly retained as internal energies of O_2 and $C_9H_{12}^+$, respectively. Mainly the resonant channel is the one affected by pressure in the present experiments. In summary, the three channels are

$$O_2^+ + C_9H_{12} \rightarrow O_2 + C_9H_{12}^+* \qquad g_a \qquad (4.1a)$$

$$O_2^+ + C_9H_{12} \rightarrow (O_2{-}C_9H_{12})^+ \rightarrow O_2 + C_9H_{12}^+* \qquad g_b \qquad (4.1b)$$

$$O_2^+ + C_9H_{12} \rightarrow O_2^*\ (^1\Delta \text{ or } ^1\Sigma) + C_9H_{12}^+ \qquad g_c \qquad (4.1c)$$

with branching fractions g_a for near-resonant charge transfer, g_b for complex-forming charge transfer, and g_c for near-resonant or complex-forming charge transfer with electronic excitation of O_2, such that $g_a + g_b + g_c = 1$.

We modeled the energy distributions $g(E,T)$ of $C_9H_{12}^+$ arising from channels 4.1a−c by analogy to ref 7. For convenience, the thermal vibrational distribution was calculated with the density functional theory (DFT) frequencies of $C_9H_{12}^+$ derived in ref 15. Employing the energy parameters from the same reference, the difference of the ionization energies of O_2 and C_9H_{12} amounts to $E_{ch}/hc = 27\,030$ cm^{-1} whereas the dissociation energy of $C_9H_{12}^+$ into $C_2H_5 + C_7H_7^+$ (benzylium) at 0 K is estimated to be $E_0/hc = 13\,950$ cm^{-1}.

This value will be of particular importance for the analysis of k_8. Figure 5 shows a representative modeling result for $g(E,$ 473 K) using $g_a = 0.60$, $g_b = 0.27$, and $g_c = 0.13$ and assuming that the $(O_2{-}C_9H_{12})^+$ complex distributes its energy statistically over the vibrations of O_2 and $C_9H_{12}^+$ and the translation and rotations of the relative motion.

Unfortunately, the available data on S/D at low and intermediate pressure are not sufficient to fix the branching ratios g_a and g_b with certainty. This prevents inclusion of a temperature

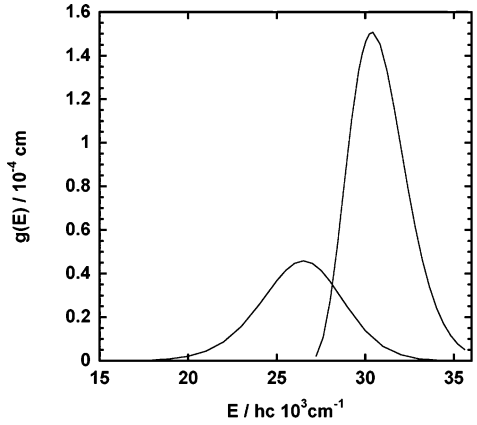

Figure 5. Energy distributions $g(E,T)$ (in $1/cm^{-1}$) of excited $C_9H_{12}^+$* from the charge transfer $O_2^+ + n\text{-}C_9H_{12}$ ($T = 473$ K, representative calculations with assumed branching ratios $g_a = 0.60$ (curve at higher energies) and $g_b = 0.27$ (curve at lower energies), see the text).

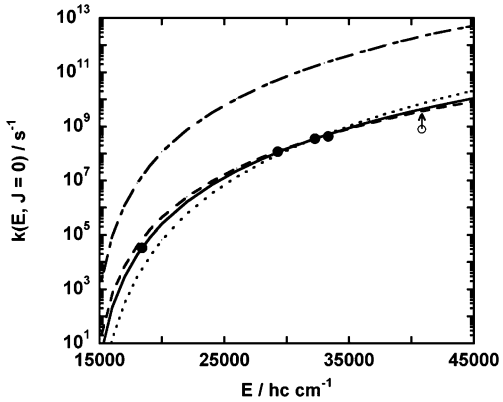

Figure 6. Specific rate constants $k(E)$ for the dissociation $C_9H_{12}^+ \rightarrow C_7H_7^+ + C_2H_5$ (experimental points from ref 15; however, see ref 15a): long−short dashed curve, PST; dashed curve, SACM/CT modeling from ref 20; dotted curve, RRKM fit from ref 15; full line, empirical representation by eq 4.3. All curves (except PST) are fine-tuned to the experimental $k(E)$ at $E/hc = 32\,260$ cm^{-1} from ref 15; see the text.

dependence. The value of $g_c \approx 0.13$ follows from the single collision results. For this reason, we cannot make an analysis which accounts for the full energy distribution $g(E,T)$. Instead, we have to limit ourselves to an analysis based on eq 3.6. It was shown in our $O_2^+ + C_8H_{10}$ study that this simplified analysis leads to an overall uncertainty of about a factor of 2 in $\langle \Delta E \rangle$. The fraction $1 - \alpha$ of channel 3.2 includes not only g_a from channel 4.1a but also the high-energy portion from channel 4.1b. Figure 5 illustrates the corresponding overlap of the distributions g_a and g_b. Isomerization was considered as a source of the intercepts but was dismissed because the temperature dependence of the intercepts would be much larger for a process with a large barrier.

4.2. Specific Rate Constants for the Dissociation of $C_9H_{12}^+$*. As the product $Z\langle \Delta E \rangle$ is derived from a relative rate measurement, its precision depends on that of the reference rate constant, that is, the specific rate constant $k(E)$ for dissociation of $C_9H_{12}^+$*, in addition to uncertainties of the energy distribution $g(E,T)$. Unfortunately, there exists experimental information on $k(E)$ only from a single study.[15] These data have been fitted by a rigid activated-complex RRKM model in ref 15, the results of which can be represented by the expression

$$k(E) = 3.6 \times 10^8\ s^{-1}\,[(E - E_0)/hc\ 18310\ cm^{-1}]^{7.776} \quad (4.2)$$

with $E_0/hc = 13\,950$ cm^{-1}. The experimental data in the range $(1-4) \times 10^8$ s^{-1}, of course, are well reproduced by eq 4.2 since they defined the fitted activated complex frequencies of the RRKM representation.

The $k(E)$ data from ref 15 were measured at energies not much above those reached in the present experiments. They are, therefore, sufficient to evaluate our measured S/D values with respect to energy transfer. However, without further considerations they cannot be used to establish a relation to the thermal dissociation rate constants. First, there is the lack of a proper account for the J-dependence of the specific rate constants, $k(E,J)$, and in particular of the threshold energies $E_0(J)$, which are essential for the calculation of the thermal rate constant, k_∞. Second, the RRKM fit corresponds to a vibrationally adiabatic treatment of the dynamics. However, it was shown in ref 20 that rigid activated complex RRKM theory does not provide an adequate approach to $k(E)$ for simple bond fission processes when the Massey parameter for the transitional mode dynamics corresponds to nonadiabatic behavior. This is particularly true for systems with transition state shifting, taking place on a potential energy surface with both long-range electrostatic and short-range valence character. The Massey parameter for the $C_9H_{12}^+$ dissociation indeed signals nonadiabatic dynamics[20] so that an RRKM treatment is good only for fitting purposes. There is an interesting apparent contradiction: on one hand, kinetic energy distributions of the fragments often are well represented by loose activated complex transition state, or phase space, theory (PST); on the other hand, specific rate constants $k(E)$ are far below PST predictions. This apparent contradiction can be resolved by realizing the nonadiabatic character of the dynamics: (1) the dissociation bottleneck governing $k(E)$ is located in the range of the potential where dynamical constraints arise from the marked anisotropy of the potential such that $k(E)$ is far below PST values; (2) nonadiabatic dynamics changes the kinetic energy distribution among the fragments beyond the bottleneck far into the range where the potential becomes increasingly isotropic such that PST applies.

In the modeling study of ref 20, we have designed long-range/short-range switching potentials and calculated $k(E,J)$ using the statistical adiabatic channel model/classical trajectory (SACM/CT) approach. Our results for ethylbenzene cation dissociation were found to be in fairly good agreement with experimental results of $k(E)$ over the range 10^3-10^8 s^{-1}. This provides confidence in the $k(E)$ for the dissociation of *n*-propylbenzene cations which was also modeled in ref 20. These modeling results could well be represented by the empirical expression

$$k(E,J{=}0) = 3.6 \times 10^8\ s^{-1}\,[(E - E_0(J{=}0))/hc\ 18310\ cm^{-1}]^{6.541} \quad (4.3)$$

Equation 4.3 is fine-tuned to the experimental values $k(E) = 3.6\ (\pm 0.4) \times 10^8$ s^{-1} at $E/hc = 32\,260$ cm^{-1}. One finds that $k(E)$ is somewhat closer to PST results at lower energies and it falls increasingly below PST at higher energies. This behavior is illustrated in Figure 6 where $k(E,J{=}0)$ from PST is compared with the RRKM fit shown in eq 4.2, the empirical expression of eq 4.3, the SACM/CT results,[20] and the experimental points.[15] Equation 4.3 has a similar energy dependence to that for $C_8H_{10}^+$ dissociation where an exponent of 4.824 was found. The larger number of medium- to low-frequency oscillators in $C_9H_{12}^+$ is responsible for the larger exponent in eq 4.3.

$C_8H_{10}^+$ and $C_9H_{12}^+$ have nearly equal dissociation energies. Because of the larger number of oscillators, one would expect that $k(E)$, at the same $E - E_0$, is smaller for $C_9H_{12}^+$ than for $C_8H_{10}^+$. However, the opposite is true: for the range of interest

in the present work, $k(E)$ apparently is about a factor of 2 larger for $C_9H_{12}^+$ than the corresponding value for $C_8H_{10}^+$. Again, the reason is that there are more medium- to low-frequency oscillators in $C_9H_{12}^+$. As a consequence, higher pressures for collisional stabilization are required in $C_9H_{12}^+$ than in $C_8H_{10}^+$. This is illustrated by comparing Figure 4 of the present work with Figure 1 of ref 7.

4.3. Collisional Energy Parameters for Excited $C_9H_{12}^+$*. An evaluation of S/D versus [M] was made in two stages as we did previously.[7] First it was assumed that the nonresonant charge transfer channels 4.1b and 4.1c only contribute to the apparent intercepts, and second, the influence of the energy distribution of channel 4.1b was taken into account. The former, a simplified analysis, was preferred in the present work. Nevertheless, we also show the results from a representative simulation of the more precise analysis. However, we are unable to fix the required parameters g_a and g_b with the same certainty that was possible for $C_8H_{10}^+$. The analysis[7] from eq 3.6 leads to the expression

$$\frac{S}{D} \approx \frac{\alpha}{1-\alpha} + \frac{Z[M](-\langle\Delta E\rangle)s^*}{(1-\alpha)k(E_{ch})(E_{ch}-E_0)}I(T) \qquad (4.4)$$

with

$$I(T) = \int_0^\infty \left(\frac{E_{ch}-E_0}{E_{ch}-E_0+E_{th}}\right)^{s^*}\left(\frac{E_{th}+E_{ch}}{E_{ch}}\right)\frac{\rho(E_{th})}{Q_{vib}}\exp\left(-\frac{E_{th}}{kT}\right)dE_{th} \qquad (4.5)$$

In this expression, we assume $k(E)$ to be of the form $k(E) \propto (E - E_0)^{s^*-1}$ used in eq 4.3, $\rho(E_{th})$ is the vibrational density of states, and Q_{vib} is the vibrational partition function of $C_9H_{12}^+$. We also assume that $\langle\Delta E\rangle$ is proportional to E and does not depend on T. The collision efficiency γ_c according to ref 10 can be related to $\langle\Delta E\rangle$ by the expression

$$\frac{\gamma_c}{1-\gamma_c^2} \approx \frac{-\langle\Delta E\rangle s^*}{E-E_0} \qquad (4.6)$$

If $\gamma_c \ll 1$, as found here, the left-hand side approaches γ_c. Table 4 includes the corresponding values for γ_c (0 K) $\approx -\langle\Delta E\rangle s^*/(E_{ch} - E_0)$ and $I(T)$. The values for $\langle\Delta E\rangle$, such as derived from the experimental values for $k(E)/\gamma_c$, are also given in this table.

The detailed analysis, accounting for near-resonant (eq 4.1a) and nonresonant (eqs 4.1b,c) charge transfer, is more involved. It has been described in ref 7 and will not be explained here again. We only illustrate the dependence of S/D on [M] by employing $g(E,T)$ from section 4.1 with representative branching ratios of $g_a \approx 0.60$, $g_b \approx 0.27$, and $g_c \approx 0.13$. Figure 7 compares this modeling with the experimental S/D versus $[N_2]$.

One realizes that there are some deviations of the experimental results from the modeled curves. We were unable to trace the origin of these deviations, in particular for the measurements at 423 K which are not included in Figure 7. In addition, the modeled S/D versus $[N_2]$ plots are more curved at low $[N_2]$ than the experimental data. The latter may indicate inadequate branching ratios g_a and g_b or problems with the statistical modeling of the charge transfer channel 4.1b. We varied g_a and g_b within this model but could not obtain much better agreement with the experiments. (Increasing $\langle\Delta E\rangle$ or decreasing g_a would have produced steeper curves of S/D versus $[N_2]$.) Therefore, we limited ourselves to the simplified analysis

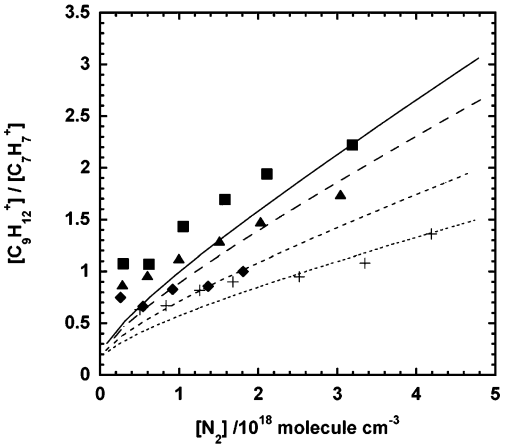

Figure 7. Modeling of the dependence of S/D on $[N_2]$ (energy distributions $g(E,T)$ from section 4.1 with representative assumed values $g_a = 0.60$, $g_b = 0.27$, and $g_c = 0.13$; experimental points as in Figure 4).

using eqs 4.4−4.6 and accept an uncertainty of the derived values of $\langle\Delta E\rangle$ of about a factor of 2.

The mean value of $\langle\Delta E\rangle$ from Table 4 is

$$\langle\Delta E\rangle/hc = -200\ (\pm 100)\ \text{cm}^{-1} \qquad (4.7)$$

at an average excitation energy of $E/hc \approx (30\,000-33\,000)$ cm^{-1}. This value of $\langle\Delta E\rangle$ is in good agreement with the corresponding result for stabilization of $C_8H_{10}^+$* in collisions with N_2 which, at a similar excitation energy, gave $\langle\Delta E\rangle/hc = -285\ (\pm 150)\ \text{cm}^{-1}$. Although there remains an uncertainty of about a factor of 2 in $\langle\Delta E\rangle$, we find again that $\langle\Delta E\rangle$ values for excited ions are similar to the corresponding $\langle\Delta E\rangle$ values for excited neutral molecules.[21−25] In contrast, the collision frequencies Z for ions and neutrals are markedly different.

4.4. Relation between Specific Rate Constants $k(E)$ and Thermal Rate Constants $k(T)$ for $C_9H_{12}^+$ Dissociation. Determining both specific rate constants $k(E)$ and thermal rate constants k_8 for the dissociation $C_9H_{12}^+ \rightarrow C_7H_7^+(Bz) + C_2H_5$ offers the rare possibility to check the internal consistency of the derived data. This analysis requires the full details of unimolecular rate theory. In particular, the contributions of angular momentum (quantum number J) in $k(E,J)$ need to be accounted for, both in energy-specific and in thermal measurements. This analysis has been done in our parallel SACM/CT study[20] where $k(E,J)$ was derived from trajectory calculations employing a model potential which was fine-tuned to reproduce the experimental measurements of $k(E)$.[15] Based on these calculations of $k(E,J)$, thermally averaged rate constants $k_{rec,\infty}(T)$ for the recombination $C_7H_7^+ + C_2H_5 \rightarrow C_9H_{12}^+$ were derived. An important result from this analysis was the demonstration that the marked difference of the calculated $k(E,J)$ from the results given by PST also occurs in the thermal rate constants: $k(E,J)$ falls increasingly below the PST results with increasing E, and $k_{rec,\infty}(T)$ analogously falls below the phase space theory results with increasing T. In other words, $k_{rec,\infty}(T)$ is expected to be much smaller than the Langevin rate constant for capture of C_2H_5 by $C_7H_7^+$. On the basis of the experimental $k(E)$ values, the recombination rate was predicted[20] to be

$$k_{rec,\infty}(T) \approx 8.0 \times 10^{-12}(T/600\ \text{K})^{-1.16}\ \text{cm}^3\ \text{molecule}^{-1}\ \text{s}^{-1} \qquad (4.8)$$

over the temperature range 400−800 K. In contrast, the Langevin rate constant is given by $k_L = 1.0 \times 10^{-9}$ cm^3 molecule^{-1} s^{-1}.

To compare the predicted $k_{rec,\infty}(T)$ with the measured k_8 from section 3, the equilibrium constant was calculated as

$$K_{eq} = ([C_7H_7^+][C_2H_5]/[C_9H_{12}^+])_{eq} = k_{diss}/k_{rec} \quad (4.9)$$

and $k_{diss,\infty}(T)$ was obtained by combining K_{eq} with $k_{rec,\infty}$. It then has to be decided whether the measured k_8 is less than the high-pressure limiting dissociation rate constant $k_{diss,\infty}$ because of falloff effects. For internal consistency, we calculated K_{eq} with the DFT frequencies from ref 15, keeping in mind that the largest uncertainty stems from the bond energy E_0 which, as before, was taken to be $E_0/hc = 13\,950$ cm^{-1}. In this way, between 500 and 600 K, we obtained

$$K_{eq} = 1.67 \times 10^{27}(T/600\text{ K})^{-0.33} \exp(-E_0/kT) \text{ molecule cm}^{-3} \quad (4.10)$$

To assess falloff effects, we calculated limiting low-pressure rate constants $k_{diss,0}$ following the conventional method described in ref 26. The relevant quantities entering $k_{diss,0}$ are $Z = 6.5 \times 10^{-10}$ cm^3 molecule^{-1} s^{-1}, $\beta_c \approx 0.2$, the vibrational density of states $\rho_{vib}(E_0) = 5.4 \times 10^{14}$/cm^{-1}, the vibrational partition function $Q_{vib}(603\text{ K}) = 8.2 \times 10^5$, $F_E(600\text{ K}) \approx 1.6$, and $F_{rot} \approx F_{rot,max}(603\text{ K}) \approx 5.3$. Combining $k_{diss,\infty} = k_{rec,\infty}K_{eq}$ from eqs 4.8−4.10 with the derived $k_{diss,0}$ indicates that the center of the falloff curve $k_{diss,0}([M]) = k_{diss,\infty}$ at 600 K is located near $[N_2]_{center} \approx 4 \times 10^{13}$ molecule cm^{-3}. Falloff curves connecting $k_{diss,0}$ with $k_{diss,\infty}$ have been illustrated in refs 26 and 27 for systems of comparable size. On this basis, one can safely assume that the measured k_8 corresponds to the high-pressure rate constant $k_{diss,\infty}$ within a few percent. The absence of an observable pressure dependence in Table 2 confirms this conclusion.

Combining the modeled $k_{rec,\infty}$ with K_{eq} from eqs 4.8−4.10 predicts

$$k_8 = 1.34 \times 10^{16}(T/600\text{ K})^{1.49} \exp(-E_0/kT)\text{ s}^{-1} \quad (4.11)$$

The prediction is remarkably close to our direct measurement of k_8 given by eq 3.7 with $E_0 = 166.9$ kJ mol^{-1}. The difference between $k_{rec,\infty}$ and $k_{Langevin}$ in the modeling has been calibrated by the difference between the measured $k(E)$ and $k(E)$ from PST such that realistic values of k_8 should have been produced. The good agreement between the measured k_8 from eq 3.7 and the predicted k_8 from eq 4.11 confirms the validity and internal consistency of the described approach. The agreement between the measured and the modeled value also supports the E_0 value of $E_0/hc = 13\,950$ cm^{-1} (or $E_0 = 166.9$ kJ mol^{-1}) used in the analysis. The difference of a factor of 1.6 in k_8 under our conditions would correspond to a difference of about 190 cm^{-1} in E_0/hc. The energetics of the dissociation $C_9H_{12}^+ \rightarrow C_7H_7^+ + C_2H_5$, therefore, should be accurate to better than about 2.2 kJ mol^{-1}.

5. Conclusions

This study described charge transfer generating excited $C_9H_{12}^+$ ions which then dissociate mainly to $C_7H_7^+$ ions and C_2H_5 radicals. Calibrating S/D ratios for chemical activation using literature values of the specific rate constants for dissociation, absolute values for collisional stabilization rates were obtained. From these quantities, average energies transferred per collision $\langle\Delta E\rangle/hc = -200\ (\pm 100)$ cm^{-1} were derived for a bath gas N_2 at excitation energies near $E/hc = 32\,000$ cm^{-1}. These values are similar to those measured for excited $C_8H_{10}^+$ ions, where $\langle\Delta E\rangle/hc = -285\ (\pm 150)$ cm^{-1} was obtained. They are also of similar magnitude as found for the corresponding excited neutral molecules.

The conversion of specific rate constants $k(E)$ into high-pressure thermal dissociation rate constants $k_{diss,\infty}(T)$ was performed by unimolecular rate theory in the form of SACM/CT calculations. As $k_{diss,\infty}(T)$ has a particularly large temperature dependence, these quantities also allowed us to confirm the dissociation energy of $C_9H_{12}^+$ as 166.9 (±2.2) kJ mol^{-1} (at 0 K). The given analysis provided an intrinsically consistent description of rate parameters such that it may serve as an example for subsequent studies of other chemical/thermal activation reactions of excited molecular ions.

Acknowledgment. This project was funded by the United States Air Force Office of Scientific Research under Project 2303EP4 and Grant Award FA8655-03-1-3034. Financial support by the Deutsche Forschungsgemeinschaft (SFB 357 "Molekulare Mechanismen unimolekularer Reaktionen") is also gratefully acknowledged.

References and Notes

(1) Williams, S.; Midey, A. J.; Arnold, S. T.; Morris, R. A.; Viggiano, A. A.; Chiu, Y.-H.; Levandier, D. J.; Dressler, R. A.; Berman, M. R. *J. Phys. Chem. A* **2000**, *104*, 10336.

(2) Arnold, S. T.; Williams, S.; Dotan, I.; Midey, A. J.; Morris, R. A.; Viggiano, A. A. *J. Phys. Chem. A* **1999**, *103*, 8421.

(3) Arnold, S. T.; Dotan, I.; Williams, S.; Viggiano, A. A.; Morris, R. A. *J. Phys. Chem. A* **2000**, *104*, 928.

(4) Viggiano, A. A.; Miller, T. M.; William, S.; Arnold, S. T.; Seeley, J. V.; Friedman, J. F. *J. Phys. Chem. A* **2002**, *106*, 11917.

(5) Midey, A. J.; Williams, S.; Arnold, S. T.; Viggiano, A. A. *J. Phys. Chem. A* **2000**, *106*, 11726.

(6) Fridgen, T. D.; McMahon, T. B.; Troe, J.; Viggiano, A. A.; Midey, A. J.; Williams, S. *J. Phys. Chem. A* **2004**, *108*, 5600.

(7) Troe, J.; Viggiano, A. A.; Williams, S. *J. Phys. Chem. A* **2004**, *108*, 1574.

(8) Kim, Y. H.; Choe, J. C.; Kim, M. *J. Phys. Chem. A* **2001**, *105*, 5751.

(9) Malow, M.; Penno, M.; Weitzel, K.-M. *J. Phys. Chem. A* **2003**, *107*, 10625.

(10) Troe, J. *J. Phys. Chem.* **1983**, *87*, 1800.

(11) Miasek, P. G.; Harrison, A. G. *J. Am. Chem. Soc.* **1975**, *97*, 714.

(12) Ahmed, M. S.; Dunbar, R. C. *J. Am. Chem. Soc.* **1987**, *109*, 3215.

(13) Barfknecht, A. T.; Brauman, J. I. *J. Chem. Phys.* **1986**, *84*, 3870. Boering, K. A.; Brauman, J. I. *J. Chem. Phys.* **1992**, *97*, 5439.

(14) Fernandez, A.; Viggiano, A. A.; Miller, T. M.; Williams, S.; Troe, J. *J. Phys. Chem.*, to be submitted.

(15) Hwang, W. G.; Moon, J. H.; Choe, J. C.; Kim, M. S. *J. Phys. Chem. A* **1998**, *102*, 7512. (a) One should note that the point with $k(E) = 3.4 \times 10^4$ s^{-1} may not be a true experimental point; its energy $E/hc = 18\,390$ cm^{-1} was "estimated from the rate−energy curve", i.e., presumably from the RRKM calculation in ref 15. However, our own RRKM calculation of $k(E)$ using the same activated complex frequencies gives values of $k(E)$ at $E/hc = 18\,390$ cm^{-1} which are markedly lower than 3.4×10^4 s^{-1}; see Figure 6.

(16) Arnold, S. T.; Seeley, J. V.; Williamson, J. S.; Mundis, P. L.; Viggiano, A. A. *J. Phys. Chem. A* **2000**, *104*, 5511.

(17) *NIST Chemistry WebBook*, http://webbook.nist.gov/chemistry.

(18) Rusyniak, M.; Ibrahim, Y.; Alsharaeh, E.; Meot-Ner (Mautner), M.; El-Shall, M. S. *J. Phys. Chem. A* **2003**, *107*, 7656.

(19) Hirschfelder, J. O.; Curtiss, C. F.; Bird, R. B. *Molecular Theory of Gases and Liquids*; J. Wiley: New York, 1964. Miller, Th. M. In *Handbook of Chemistry and Physics*; Lide, D. R., Ed.; CRC Press: Boca Raton, FL, 2003; Section 10, p 163.

(20) Troe, J.; Ushakov, V. G.; Viggiano, A. A.; Williams, S. *J. Chem. Phys.*, to be submitted.

(21) Hold, U.; Lenzer, Th.; Luther, K.; Reihs, K.; Symonds, A. C. *J. Chem. Phys.* **2000**, *112*, 4090.

(22) Lenzer, Th.; Luther, K.; Reihs, K.; Symonds, A. C. *J. Chem. Phys.* **2000**, *112*, 4090.

(23) Grigoleit, U.; Lenzer, Th.; Luther, K.; Mützel, M.; Takahara, A. *Phys. Chem. Chem. Phys.* **2001**, *3*, 2191.

(24) Troe, J.; Wieters, W. *J. Chem. Phys.* **1979**, *71*, 3931.

(25) Hippler, H.; Luther, K.; Troe, J.; Wendelken, H. J. *J. Chem. Phys.* **1983**, *79*, 239.

(26) Troe, J. *J. Phys. Chem.* **1979**, *83*, 114.

(27) Troe, J.; Ushakov, V. G. *Faraday Discuss.* **2001**, *119*, 145.

(28) Hamon, S.; Speck, T.; Mitchell, J. B. A.; Rowe, B. R.; Troe, J. *J. Chem. Phys.* **2002**, *117*, 2557.